Dissociative recombination and vibrational excitation of BF$^+$ in low energy electron collisions

J. Zs. Mezei[1,2,3,4], **F. Colboc**[1], **N. Pop**[5], **S. Ilie**[1,5], **K. Chakrabarti**[1,6], **S. Niyonzima**[7], **M. Lepers**[2], **A. Bultel**[8], **O. Dulieu**[2], **O. Motapon**[9], **J. Tennyson**[10], **K. Hassouni**[4], and **I. F. Schneider**[1,2]

[1]Laboratoire Ondes et Milieux Complexes CNRS−Université du Havre−Université Normandie, 76058 Le Havre, France
[2]Laboratoire Aimé-Cotton, CNRS−Université Paris-Sud−ENS Cachan−Université Paris-Saclay, 91405 Orsay, France
[3]Institute of Nuclear Research of the Hungarian Academy of Sciences, P.O. Box 51, H-4001 Debrecen, Hungary
[4]Laboratoire des Sciences des Procédés et des Matériaux, CNRS−Université Paris 13−USPC, 93430 Villetaneuse, France
[5]Department of Fundamental of Physics for Engineers, Politehnica University of Timisoara, Bv. V. Parvan No.2, 300223 Timisoara, Romania
[6]Dept. of Mathematics, Scottish Church College, 1 & 3 Urquhart Sq., Kolkata 700 006, India
[7]Département de Physique, Faculté des Sciences, Université du Burundi, B.P. 2700 Bujumbura, Burundi
[8]CORIA CNRS−Université de Rouen−Université Normandie, F-76801 Saint-Etienne du Rouvray, France
[9]LPF, UFD Mathématiques, Informatique Appliquée et Physique Fondamentale, University of Douala, P. O. Box 24157, Douala, Cameroon
[10]Dept. of Physics and Astronomy, University College London, London WC1E 6BT, UK

E-mail: `janos.mezei@univ-lehavre.fr`

Abstract. The latest molecular data - potential energy curves and Rydberg-valence interactions - characterising the super-excited electronic states of BF are reviewed in order to provide the input for the study of their fragmentation dynamics. Starting from this input, the main paths and mechanisms of BF$^+$ dissociative recombination and vibrational excitation are analysed. Their cross sections are computed for the first time using a method based on the multichannel quantum defect theory (MQDT), and Maxwellian rate-coefficients are calculated and displayed in ready-to-be-used format for low temperature plasma kinetics simulations.

1. Introduction

Boron fluoride (BF$_3$) containing plasmas are important for applications in the field of material processing. BF$_3$ and Ar/BF$_3$ plasmas are for instance used for p-type doping in the semi-conductor industry (Torregrosa *et al* 2004, Matsui *et al* 2004). Moreover, electrical discharges generated in complex mixture of BF$_3$ with nitrogen containing compounds have been proposed and investigated for the deposition of boron nitride coatings (Yu & Matsumoto 2003, Yamamoto *et al* 2006). All these processes make use of low pressure high density plasma sources where BF$_3$ interacts with the free electrons of the plasma through elastic and inelastic collisions. These collisions are not only the driver for the generation of the active key-species of the process, e.g., the positive ions for the plasma immersion ion implantation (PIII) doping processes or active radicals for the deposition processes, but they also contribute and govern the discharge equilibrium and stability through ionisation, attachment and recombination processes (Agarwal &Kushner 2007, Farber & Srivastava 1984, Kim & Irikura 2000). In particular, for high density magnetised inductively coupled radio-frequency sources used in many of these processes, the surface losses are limited due to the magnetic confinement, which makes the contribution of ion recombination and mutual recombination processes to the discharge equilibrium very significant. In this context, the BF$^+$ ion can represent a significant fraction of the ions produced when working at high power density discharge conditions for which BF$_3$ dissociation and dissociative ionisation are strongly enhanced and the plasma is dominated by BF$_2$ and BF fragments (Maury *et al* 2016). These species can therefore significantly contribute either as an active species in the processes or in the discharge ionisation-recombination equilibrium. The investigation of the dissociative recombination of BF$^+$ is therefore of importance for understanding BF$_3$ plasma processes.

The kinetic description of all the above mentioned environments is based on the knowledge of the rate coefficients of the dominant reactions, including those between electrons and molecular ions. As for the BF$^+$ ions, their abundance and their vibrational distribution are strongly affected by the dissociative recombination (DR),

$$\text{BF}^+(v_i^+) + e^- \rightarrow \text{B} + \text{F}, \tag{1}$$

and also by other competitive processes, such as inelastic collisions ($v_f^+ > v_i^+$) and super-elastic collsions ($v_f^+ < v_i^+$) which are also known as collisions of the second kind:

$$\text{BF}^+(v_i^+) + e^- \rightarrow \text{BF}^+(v_f^+) + e^-, \tag{2}$$

where v_i^+ and v_f^+ stand for the initial and final vibrational quantum number of the target ion, and rotational structure is neglected.

In the present work, we compute the DR and vibrational transition (VT) - vibrational excitation/de-excitation (VE/VdE) - cross sections and rate coefficients for the lowest three vibrational levels of the BF$^+$ in its ground electronic state using the multichannel quantum defect theory (MQDT). The paper is structured as follows: Section 2 outlines the main ideas and steps of our MQDT approach. Section 3 presents the molecular data used in the calculation. The main results are given in section 4 and the paper ends by conclusions.

2. The MQDT-type approach to DR

The MQDT approach (Seaton 1983, Greene and Jungen 1985, Jungen 1996, Giusti-Suzor 1980) has been shown to be a powerful method for the evaluation of the cross sections in collisions of electrons/photons with molecular cation/neutral systems. It was applied with great success in calculating DR cross sections to several diatomic systems like H_2^+ and its isotopologues (Giusti-Suzor *et al* 1983, Schneider *et al* 1991, Takagi 1993, Tanabe *et al* 1995, Schneider *et al* 1997, Amitay *et al* 1999), O_2^+ (Guberman and Giusti-Suzor 1991, Guberman 2000), NO^+ (Sun and Nakamura 1990, Vâlcu *et al* 1998, Schneider *et al* 2000a) and triatomics like H_3^+ (Schneider *et al* 2000b, Kokoouline *et al* 2001, Kokoouline and Greene 2003), and for its competitive processes like ro-vibrational transitions in case of NO^+ (Motapon *et al* 2006), CO^+ (Mezei *et al.* 2015) and H_2^+ (Ngassam *et al* 2003a, Epée Epée *et al* 2015). Recently, a global version of MQDT (Jungen 2011) has been used to describe the photoabsorption, photoionisation and photodissociation of H_2 (Mezei *et al* 2012, Mezei *et al* 2014, Sommavilla *et al* 2016), providing very good agreement with highly accurate experimental results.

In the present paper, we use an MQDT-type method to study the electron-impact collision processes given by eqs. (1) and (2) which result from the quantum interference of the *direct* mechanism - the capture takes place into a dissociative state of the neutral system (BF^{**}) - and the *indirect* one - the capture occurs *via* a Rydberg state of the molecule BF^* which is predissociated by the BF^{**} state. In both mechanisms the autoionization is in competition with the predissociation and leads, through the reaction (2), to *super-elastic collision* (SEC) ($v_i^+ > v_f^+$ in eq. (2)), *elastic collision* (EC) ($v_i^+ = v_f^+$) and *inelastic collision* (IC) ($v_i^+ < v_f^+$).

A detailed description of our theoretical approach is given in previous studies (Little *et al* 2014, Mezei *et al.* 2015). The major steps of the method only can be briefly outlined as follows:

(i) *Defining the interaction matrix* $\mathcal{V}$:
Within a quasi-diabatic representation of the BF states, the interaction matrix is based on the computed (Chakrabarti and Tennyson 2009, Chakrabarti *et al* 2011) couplings between *ionisation* channels - associated to the vibrational levels v^+ of the cation and to the orbital quantum number l of the incident/Rydberg electron - and *dissociation* channels d_j.

(ii) *Computation of the reaction matrix* $\mathcal{K}$:
Given H_0 the Hamiltonian of the molecular system under study in which the Rydberg-valence interaction is neglected, we adopt the second-order perturbative solution for the Lippman-Schwinger integral equation (Ngassam *et al* 2003a, Florescu *et al* 2003, Motapon *et al* 2006), written in operatorial form as:

$$\mathcal{K} = \mathcal{V} + \mathcal{V}\frac{1}{E - H_0}\mathcal{V}. \tag{3}$$

(iii) *Diagonalization of the reaction matrix,*
yields the corresponding eigenvectors and eigenvalues which are used to build the eigenchannel wavefunctions.

(iv) *Frame transformation from the Born-Oppenheimer (short-range) to the close-coupling (long-range) representation,*
relying, for a given electronic total angular momentum quantum number Λ and a given orbital quantum number of the incident/Rydberg electron l, on the quantum defect $\mu_l^\Lambda(R)$ and on the eigenvectors and eigenvalues of the K-matrix.

(v) *Construction of the generalised scattering matrix* X,
based on the frame-transformation coefficients, this matrix being organised in blocks associated to open and/or closed (o and/or c respectively) channels:

$$X = \left(\begin{array}{cc} X_{oo} & X_{oc} \\ X_{co} & X_{cc} \end{array} \right). \tag{4}$$

(vi) *Construction of the generalised scattering matrix* $\mathcal{S}$,

$$S = X_{oo} - X_{oc}\frac{1}{X_{cc} - \exp(-i2\pi\nu)}X_{co}. \tag{5}$$

based on the open channels, the first term in eq. (5), but also on their mixing with the closed ones, given by the second term, the denominator being responsible for the resonant patterns in the shape of the cross section (Seaton 1983). Here the matrix $\exp(-i2\pi\nu)$ is diagonal and contains the effective quantum numbers ν_{v^+} associated to the vibrational thresholds of the closed ionisation channels.
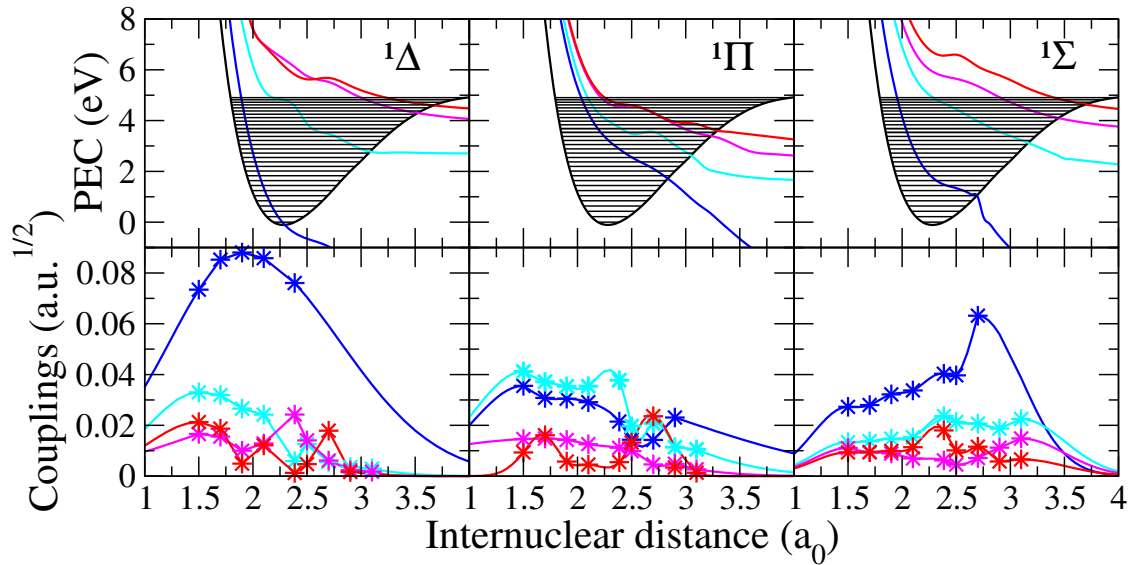
(vii) *Computation of the cross-sections:*
For each of the relevant BF states, which are grouped by symmetry properties: electronic total angular momentum quantum number Λ, electronic spin singlet/triplet, and for a given target cation vibrational level v_i^+ and energy of the incident electron ε, the dissociative recombination and the vibrational excitation/de-excitation cross sections are computed using, respectively:

$$\sigma_{\text{diss}\leftarrow v_i^+}^{\text{sym}} = \frac{\pi}{4\varepsilon}\rho^{\text{sym}}\sum_{l,j} | S_{d_j, lv_i^+} |^2, \tag{6}$$

$$\sigma_{v_f^+ \leftarrow v_i^+}^{\text{sym}} = \frac{\pi}{4\varepsilon}\rho^{\text{sym}}\sum_{l,l'} | S_{l'v_f^+, lv_i^+} - \delta_{l'l}\delta_{v_i^+ v_f^+} |^2, \tag{7}$$

where ρ^{sym} stands for the ratio between the multiplicity of the involved electronic states of BF and that of the target, BF^+.

Figure 1. The dissociative states and electronic couplings relevant for BF$^+$ dissociative recombination within the major symmetries, indicated in each figure. Top panel: the potential energy curves of the dissociative BF** states (colour, cf section 3), the ground state potential energy curve of BF$^+$ and its vibrational levels (black). Bottom panel: couplings between the valence BF** dissociative states and the ionisation continua BF$^+$ + e$^-$.

3. Molecular data

The molecular data necessary to model the DR are the potential energy curve (PEC) of the ground state of the ion, the PECs of the neutral valence dissociative states interacting with the ionization continua, those of the Rydberg states associated to these continua below the threshold, and all the relevant Rydberg-valence couplings. These molecular data are mostly obtained from *ab initio* R-Matrix calculations. In order to extend the PECs to small and large values of the internuclear distance R, we used the quantum chemistry molecular data of Magoulas *et al* (2013).

3.1. Ab initio R-Matrix calculations for the molecular states

Ab initio R-matrix calculations of electron collision with the BF$^+$ ion yielding the relevant molecular data were performed by three of us (Chakrabarti and Tennyson 2009, Chakrabarti *et al* 2011). The R-matrix method is a state-of-the-art quantum scattering technique which can be used to calculate the properties of bound and resonant electronic states of a molecule (Tennyson 2010). The BF$^+$ target states were first obtained by performing a configuration interaction (CI) calculation. Subsequently this CI target wave function was used in an R-matrix calculation. The bound states of the BF molecule were obtained by searching for negative energy solutions using the BOUND program available within the R-Matrix code suite (Sarpal et al. 1991, Carr *et al* 2012). This also produces quantum defects of the bound states. Resonances were detected and fitted to a Briet-Wigner profile (Tennyson & Noble 1984) to obtain their energies and widths. Subsequently the electronic couplings $V_{d_j,l}$ were obtained from the resonance widths $\Gamma_{d_j,l}$ using the relation
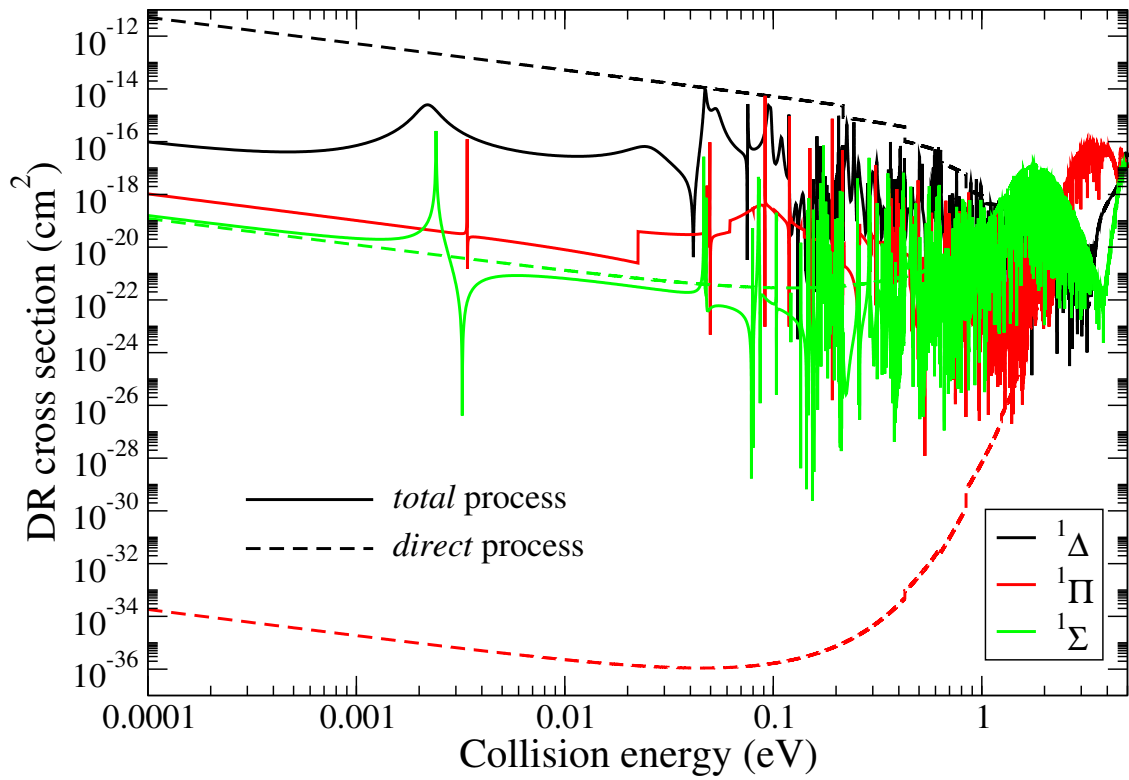
$$V_{d_j,l} = \sqrt{\frac{\Gamma_{d_j,l}}{2\pi}}. \tag{8}$$

The calculations were repeated for 11 internuclear distances in the range $1.5\ a_0 - 3.5\ a_0$. While the R-matrix calculations used several partial waves l to represent the scattering, one single generic partial wave for each symmetry was considered to take in charge the total strength of the Rydberg-valence interaction in the current calculations. Dissociative curves were constructed using the resonance data above the ion PEC and their continuation as bound states below the ion PEC.

3.2. Modeling of the potential energy curves and electronic couplings

Our earlier studies on molecular systems such as H$_2$ (Epée Epée *et al* 2015), HD (Motapon *et al* 2014), NO (Motapon *et al* 2006), N$_2$ (Little *et al* 2014) and CO (Mezei *et al.* 2015) revealed that accurate and complementary R-matrix and quantum chemistry calculations are needed for a reliable description of the molecular dynamics in electron/molecular cation collisions. In particular, we found that the DR cross section is extremely sensitive to the position of the PECs of the neutral dissociative states with respect to that of the target ion. Indeed, a slight change of the crossing point of the PEC of a neutral dissociative state with that of the ion ground state can lead to a significant change in the predicted DR cross section. In addition, the PECs of the dissociative states must also go to the correct asymptotic limits for large values of the internuclear distance R.

In order to fulfil these accuracy criteria, we smoothly matched the PECs corresponding to R-matrix resonances, situated above the ion PEC, to branches of adiabatic PECs coming from previous quantum chemistry calculations (Magoulas *et al* 2013). Some of these latter PECs allowed us to complete the relevant diabatic landscape. More specifically, since for the states having $^1\Sigma^+$ and $^1\Pi$ symmetry the avoided crossings involved always two adiabatic states only, the adiabatic PECs can be a transformed into (quasi-)diabatic PECs using a 2×2 rotation matrix (Roos *et al* 2009). Meanwhile, far from the avoided crossing, we assumed that the adiabatic and diabatic potential curves are identical. This assumption forces the rotational angle to be a function

Figure 2. DR cross section for the direct (dashed lines) and the total (direct and indirect) processes (continuous lines) for each symmetry, with the ion initially in $v_i^+ = 0$,

that varies steeply from 0 to $\pi/2$, chosen in the present case a tangent hyperbolic function. In this way we were able to extract the diabatic PECs for the dissociative states with singlet symmetries relevant for DR.

The electronic couplings provided by the R-matrix theory (Chakrabarti *et al* 2011) for the triplet states are at least one or even two orders of magnitude smaller then those of the singlet ones, so they are omitted in the present calculation.

The data on the PECs are limitted to internuclear distances with $R \leq 8 \ a_0$. We completed the diabatic PECs by adding a long-range tail of $D - \sum_n C_n/R^n$ type (Stone 1996, Lepers and Dulieu 2011) for larger values of R, where D is the dissociation limit as given in the (NIST Atomic Spectra Database 2016). For the ground state of BF$^+$, the leading term C_3/R^3 of the multipolar expansion comes from the interaction between the charge of B$^+$ and the quadrupole moment of fluorine in its ground state $^2P^o(M_L = 0)$, with M_L the azimuthal quantum number of F with respect to the internuclear axis. The corresponding coefficient $C_3 = Q = 0.731$ a.u. (Medved *et al* 2000) gives rise to a repulsive interaction, which is balanced by the next term C_4/R^4 of the multipolar expansion, due to the polarisation of the electronic cloud of F by the ion B^+. The coefficient is given by $C_4 = -\alpha_{zz}/2 = -1.72$ a.u., where $\alpha_{zz} = 3.43$ a.u. (Medved *et al* 2000) is the static dipole polarisability of the ground state $^2P^o(M_L = 0)$ of fluorine. As for the states of the BF , the C_n coefficients are calculated as fitting parameters to ensure a smooth connection with the existing part of the PECs.

The top panel of Figure 1 shows the PEC of the ion ground state - together with its vibrational structure - and the PECs of the DR-relevant dissociative states obtained using the procedure outlined above and taken into account in the present MQDT calculation. The electronic couplings of these latter states with the ionization continua, computed from the R-Matrix-produced autoionization widths followed by Gaussian-type extrapolations to small and large internuclear distances, are shown in the bottom panel of the same figure.
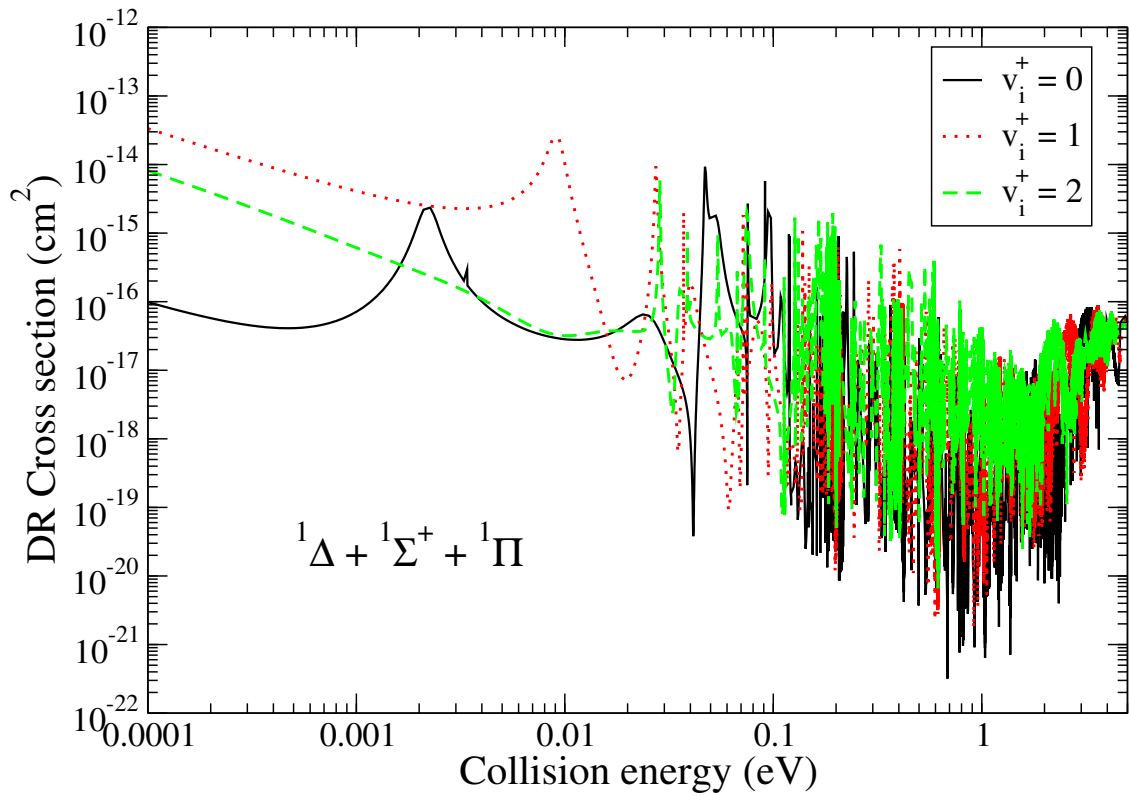
4. Results and discussion

4.1. Evaluation of the cross section using the MQDT approach

Using the set of molecular data (PECs, electronic couplings and quantum defects) determined as described in the previous section, we performed a series of MQDT calculations of cross sections for DR and competitive processes, assuming BF$^+$ to be initially in its electronic ground state X $^2\Sigma^+$ and on one of its lowest vibrational levels $v_i^+ = 0, 1$ and 2. We have considered that the reactive processes take place via BF-states of total symmetry of $^1\Delta$, $^1\Pi$, $^1\Sigma^+$ - see Figure 1 - and we neglected rotational and spin-orbit effects.

We consider incident electron energies from 0.01 meV up to 5 eV - the dissociation energy of BF$^+$ X $^2\Sigma^+$ electronic state - and all the 30 vibrational levels of the ion are included in the calculations.

At very low energy, all the excited levels are associated with closed ionisation channels, as defined in section 2, responsible for temporary resonant capture into Rydberg states. As the energy increases, more and more ionisation channels open, which results in autoionization, leading to competitive processes, such as IC and SEC, and decreasing the flux of DR.

The direct electronic couplings between ionisation and dissociation channels - mentioned in paragraph (i) of section 2 - were extracted from the autoionization widths (see eq. (8)) of the valence states calculated by Chakrabarti and Tennyson (2009).

Figure 3. Total DR cross sections for different initial vibrational levels of the ion, for all of the symmetries considered. Black continuous lines are for DR from $v_i^+ = 0$, while the red dotted and green dashed lines are for DR from $v_i^+ = 1$ and 2, respectively.

For each dissociation channel available, we considered interaction with the most relevant series of Rydberg states including only one partial wave for each symmetry.

By examining the magnitude of the valence-Rydberg couplings (shown in the bottom panel of figure 1) and the positions of the crossing points between the dissociative states correlating to the $B(2p^1) + F(2p^5)$ atomic limits with the ionic ground state - blue and black curves in the first figure of the upper panel of the same figure - at low collision energies (up to 1 eV) one may predict that the major part of the total cross section comes from the $^1\Delta$ symmetry (solid black line in figure 2), while the $^1\Sigma$ and $^1\Pi$ symmetries (solid green and red lines in the same figure) only make a minor contribution to the cross section. The importance of these latter two symmetries is revealed at higher collision energies, when the crossing of the first dissociative state with the molecular ion becomes favorable. At collision energies about 1 eV, the $^1\Sigma^+$ states give a larger contribution to the DR cross section than the $^1\Delta$ symmetry, which in turn is exceeded by the $^1\Pi$ symmetry at about 2 eV. Moreover, one can notice that at higher collision energies, around 3.5 eV, when all the dissociative states are open, the DR cross section shows a sharp revival and, at 5 eV, the resonance structures disappear since all the ionization channels are open, and consequently the direct process only drives the DR.

Figure 2 shows the importance of the *indirect* process for the DR of vibrationally relaxed BF$^+$ at low energies.

Within the $^1\Delta$ symmetry, the entrance ionization channel associated with the $v_i^+ = 0$ state is strongly coupled to the dissociation continuum (see Figure 1), allowing the direct process to dominate. The indirect process diminishes the cross section - *destructive* interferences with the direct one - due to stronger coupling between closed channels associated with highly-excited vibrational levels - $v^+ = 12 - 16$ - and the dissociative ones.
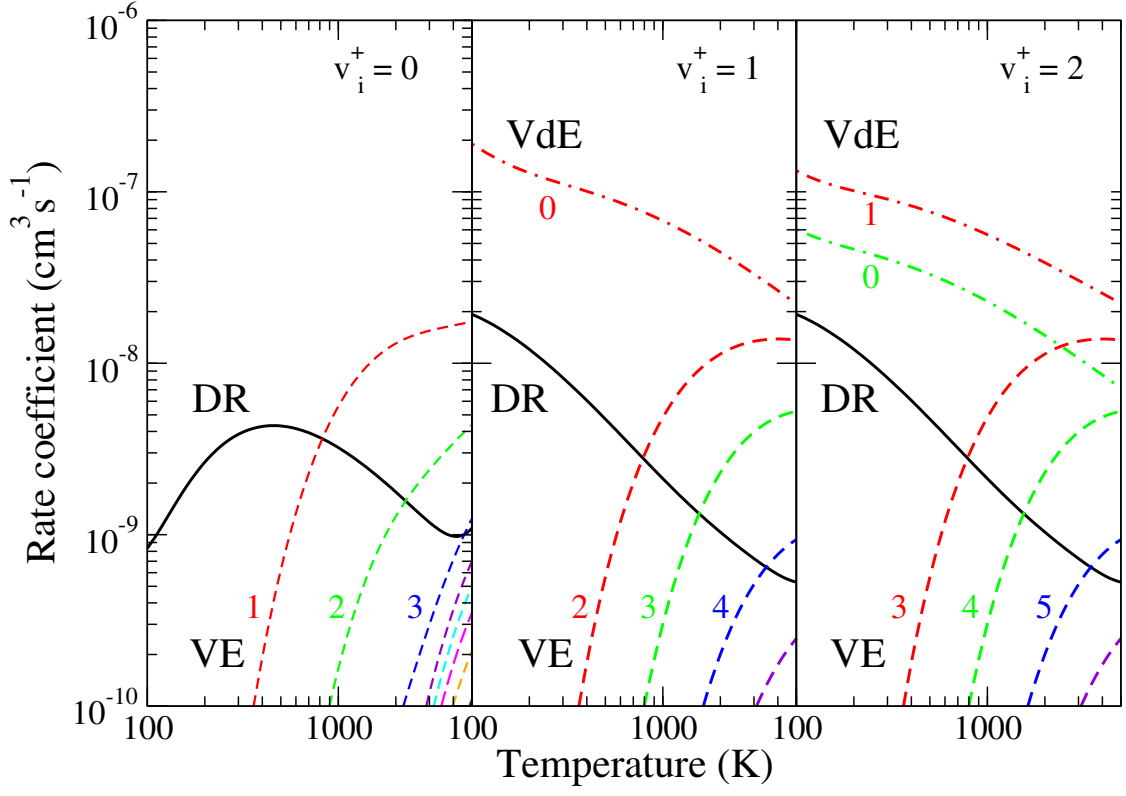
Within the $^1\Pi$ symmetry one finds the opposite. The direct process gives only a minor contribution to the DR cross section, due to the poor Franck-Condon overlap between the vibrational wave function of the initial state of the ion and the dissociative neutral states. However, the much stronger couplings between some closed ionisation channels - $v^+ = 8 - 10$ - and the dissociative states significantly increases the total cross section through the indirect mechanism (Pop *et al* 2012, Schneider *et al* 2012) resulting into *constructive* quantum interferences.

Finally, for the states with $^1\Sigma^+$ symmetry, the indirect process plays a relatively minor role, the magnitude of the total cross section being given mainly by the direct process. The indirect process is responsible for resonant structures which are a consequences of both constructive and destructive interference.

For a given initial vibrational level of BF$^+$, the total DR cross section is obtained by summing over the partial cross sections of the three symmetries contributing to the process - $^1\Delta$, $^1\Pi$ and $^1\Sigma^+$ - given in eq, (6). The results of the calculations performed for the lowest three vibrational levels of the ground electronic state of the ion are shown in Figure 3.

4.2. Reaction rate coefficients for DR and its competitive processes

Besides the dissociative recombination cross sections presented in Figure 3, we use eq. (7) to calculate the vibrational excitation (VE) and de-excitation (VdE) cross sections for the same vibrational levels of the target. Since many of the features of the VE and VdE cross sections either are similar to, or may be understood with the same reasoning as those of DR, we do not display them here. Instead, we present in this section their Maxwell rate coefficients for a broad range of electronic temperatures, in

Figure 4. DR and state-to-state VE and VdE Maxwell rate coefficients of BF^+ in its ground electronic state, v_i^+ standing for the initial vibrational quantum number of the target ion. Curves of the same color show the rate coefficients for the vibrational (de-)excitations corresponding to the same $|\Delta v| = |v_f^+ - v_i^+|$; $v_f^+ > v_i^+$ for the VE and $v_f^+ < v_i^+$ for the VdE global rate coefficients. The final vibrational quantum numbers of the ion are indicated for these processes.

comparison with those of the DR. All these data are relevant for cold non-equilibrium plasmas.

Figure 4 shows the total DR and vibrational transition - VE and VdE - rate coefficients for the three lowest vibrational levels of the ion. The DR rate for $v_i^+ = 0$ shows different behaviour to those for the $v_i^+ = 1$ and 2 states. It has a maximum at an electron temperature T_e of about 400 K, while the rates for the other two states are monotonically decreasing with T_e, reaching nearly the same magnitude at higher temperatures. This behaviour for $v_i^+ = 0$ comes from the strong resonant peaks just below 0.01 eV, see Figure 2 and black curve in Figure 3.

For other recently studied molecular systems, N_2 (Little *et al* 2014) and CO (Mezei *et al.* 2015), the DR clearly dominates the electron-ion collisions. However, for BF the calculated VdE rate coefficients are larger than the DR-ones, and VE rate coefficients exceed the DR-ones at high T_e by almost an order of magnitude. Thus, one can conclude that in the case of the BF^+ containing plasma, the internal vibrational energy is much more important for energy-exchange via VE and VdE, than the kinetic energy release via the exothermic DR.

To facilitate the use of our rate coefficients (Figure 4) in modeling calculations, we fit them using modified Arrhenius-type formulas. The calculated DR rate coefficients for $v = 0, 1, 2$ are given by :

$$k_{BF^+,v}^{DR}(T_e) = A_v T_e^{\alpha_v} \exp\left[-\sum_{i=1}^{7} \frac{B_v(i)}{i \cdot T_e^i}\right] \tag{9}$$

over the electron temperature range 100 K$<T_e<$ 3000 K. The parameters A_v, α_v, and $B_v(i)$ are listed in table 1. The corresponding formula for the vibrational transitions (VE and VdE) has the form:

$$k_{BF^+,v'\to v''}^{DR}(T_e) = A_{v'\to v''} T_e^{\alpha_{v'\to v''}} \exp\left[-\sum_{i=1}^{7} \frac{B_{v'\to v''}(i)}{i \cdot T_e^i}\right] \tag{10}$$

over the electron temperature range $T_{min}<T_e<$ 3000 K. The parameters T_{min}, $A_{v'\to v''}$, $\alpha_{v'\to v''}$, and $B_{v'\to v''}(i)$ for $i = 1, 2, \dots, 7$ are given in tables 2-4.

Table 1. Parameters used in equation (9) to represent the DR rate coefficient of BF^+. Powers of 10 are given in square brackets.

v	A_v	α_v	$B_v(1)$	$B_v(2)$	$B_v(3)$	$B_v(4)$	$B_v(5)$	$B_v(6)$	$B_v(7)$
0	0.703050632[−5]	-0.108298227[1]	-0.363984388[2]	0.68522753[6]	-0.341534791[9]	0.86262362[11]	-0.117919938[14]	0.821543800[15]	-0.229194862[17]
1	0.205402433[−11]	0.557133316[0]	-0.185580405[4]	0.110399946[7]	-0.316387400[9]	0.531242790[11]	-0.525109108[13]	0.283203635[15]	-0.643843159[16]
2	0.144845145[−5]	-0.806777388[0]	0.285629778[4]	-0.322036339[7]	0.160926033[10]	-0.409338097[12]	0.558087964[14]	-0.388815002[16]	0.108682270[18]

6

Table 2. Parameters used in equation (10) to represent the VE rate coefficient of BF$^+$ ($v = 0$). Powers of 10 are given in square brackets.

$v' \rightarrow v''$	T_{min}(K)	$A_{v' \rightarrow v''}$	$\alpha_{v' \rightarrow v''}$	$B_{v' \rightarrow v''}(1)$	$B_{v' \rightarrow v''}(2)$	$B_{v' \rightarrow v''}(3)$	$B_{v' \rightarrow v''}(4)$	$B_{v' \rightarrow v''}(5)$	$B_{v' \rightarrow v''}(6)$	$B_{v' \rightarrow v''}(7)$
$0 \rightarrow 1$	100	0.262533924[−5]	-0.547999875[0]	0.214096395[4]	0.639318590[6]	-0.338435157[9]	0.871079196[11]	-0.119891991[14]	0.844485990[15]	-0.238785179[17]
$0 \rightarrow 2$	250	0.173038633[−11]	0.899303013[0]	-0.154506863[4]	0.103113831[8]	-0.802809891[10]	0.345037537[13]	-0.831154448[15]	0.104995341[18]	-0.541063017[19]
$0 \rightarrow 3$	350	0.228322632[−19]	0.298753871[1]	0.362608159[4]	-0.187052923[8]	0.462415666[11]	-0.437428769[14]	0.208086587[17]	-0.496004570[19]	0.471734143[21]
$0 \rightarrow 4$	500	0.117098647[13]	-0.484209878[1]	0.440674967[5]	-0.535140469[8]	-0.648699676[9]	0.669344086[14]	-0.628654524[17]	0.237907644[20]	-0.333577789[22]
$0 \rightarrow 5$	700	0.409903965[−3]	-0.115252435[1]	0.195259810[5]	-0.556269189[7]	0.845592131[10]	-0.259895652[14]	0.300647776[17]	-0.147809013[20]	0.269130250[22]
$0 \rightarrow 6$	1000	0.208106654[−4]	-0.886590160[0]	0.164181737[5]	0.130228539[8]	-0.448925166[11]	0.652593625[14]	-0.524133410[17]	0.227101018[20]	-0.413751683[22]
$0 \rightarrow 7$	1000	0.191744424[−4]	-0.916885978[0]	0.176354084[5]	0.715839067[7]	-0.242161884[11]	0.338962077[14]	-0.251630983[17]	0.964448872[19]	-0.147532452[22]

Table 3. Parameters used in equation (10) to represent the VE rate coefficient of BF$^+$ ($v = 1$). Powers of 10 are given in square brackets.

$v' \rightarrow v''$	T_{min}(K)	$A_{v' \rightarrow v''}$	$\alpha_{v' \rightarrow v''}$	$B_{v' \rightarrow v''}(1)$	$B_{v' \rightarrow v''}(2)$	$B_{v' \rightarrow v''}(3)$	$B_{v' \rightarrow v''}(4)$	$B_{v' \rightarrow v''}(5)$	$B_{v' \rightarrow v''}(6)$	$B_{v' \rightarrow v''}(7)$
$1 \rightarrow 0$	100	0.452471923[−4]	-0.870739533[0]	0.482355385[3]	-0.159745070[6]	0.206190286[8]	-0.357598119[9]	-0.236882495[12]	0.278880714[14]	-0.100143557[16]
$1 \rightarrow 2$	100	0.206894707[−4]	-0.534102059[0]	0.240138665[4]	0.240026523[6]	-0.118750781[9]	0.294642142[11]	-0.398661667[13]	0.277400105[15]	-0.775646365[16]
$1 \rightarrow 3$	500	0.132913428[3]	-0.796311915[0]	0.528489192[4]	-0.227298093[6]	0.992018062[8]	-0.246177290[11]	0.334949142[13]	-0.234694329[15]	0.661421602[16]
$1 \rightarrow 4$	1000	0.618690809[−3]	-0.105997410[1]	0.102015058[5]	-0.102556918[8]	0.227295645[11]	-0.322366448[14]	0.285015517[17]	-0.142527673[20]	0.306796130[22]
$1 \rightarrow 5$	1000	0.195393605[−5]	-0.554467702[0]	0.874898467[4]	0.410394065[7]	-0.950355092[10]	0.129851249[14]	-0.110278414[17]	0.546465683[19]	-0.120534084[22]
$1 \rightarrow 6$	1500	0.144480570[27]	-0.772731693[1]	0.121808074[6]	-0.696758177[9]	0.243696228[13]	-0.508560332[16]	0.633554530[19]	-0.436110956[22]	0.127890210[25]

Table 4. Parameters used in equation (10) to represent the VE rate coefficient of BF$^+$ ($v = 2$). Powers of 10 are given in square brackets.

$v' \rightarrow v''$	T_{min}(K)	$A_{v' \rightarrow v''}$	$\alpha_{v' \rightarrow v''}$	$B_{v' \rightarrow v''}(1)$	$B_{v' \rightarrow v''}(2)$	$B_{v' \rightarrow v''}(3)$	$B_{v' \rightarrow v''}(4)$	$B_{v' \rightarrow v''}(5)$	$B_{v' \rightarrow v''}(6)$	$B_{v' \rightarrow v''}(7)$
$2 \rightarrow 0$	100	0.206905711[−4]	-0.534094193[0]	-0.522292591[2]	0.239747229[6]	-0.118624395[9]	0.294301198[11]	0.235044551[13]	0.277059236[15]	-0.774678282[16]
$2 \rightarrow 1$	100	0.281749676[−3]	-0.939661066[0]	0.573963533[3]	-0.266713211[6]	0.925188414[8]	-0.195045354[11]	-0.831154448[15]	-0.149951574[15]	0.392910054[16]
$2 \rightarrow 3$	200	0.677540315[−6]	-0.180526927[0]	0.165713437[4]	0.786441694[6]	-0.355111141[9]	0.865145438[11]	-0.110403668[14]	0.586781113[15]	-0.159145807[16]
$2 \rightarrow 4$	500	0.312513647[−2]	-0.113354017[1]	0.791543066[4]	-0.692210036[7]	0.883457770[10]	-0.684463255[13]	0.319179702[16]	-0.822026586[18]	0.896873812[20]
$2 \rightarrow 5$	1000	0.641993202[−3]	-0.101279417[1]	0.931521134[4]	-0.338959607[7]	0.140747992[10]	0.325809186[13]	-0.558558120[16]	0.350923558[19]	-0.820376383[21]

5. Conclusion

This paper presents a theoretical study of the dissociative recombination of BF$^+$ and of its competitive processes - vibrational excitation and de-excitation - over a broad range of electron energies - up to about 5 eV - and considering all the relevant dissociative states within different symmetries. Our MQDT dynamical approach is relying on molecular data calculated by the *ab initio* R-matrix method, completed by quantum chemical results. The computed Maxwell rate coefficients are relevant for the kinetic modelling of molecule based cold non-equilibrium plasmas, in the context of complete lack of other theoretical or experimental data on these processes for this cation.

The present calculations complete our very recent studies of the DR performed on N$_2^+$ (Little *et al* 2014) and on CO$^+$ (Mezei *et al.* 2015) based on fully *ab initio* potential energy curves and couplings computed with the R-matrix method (Tennyson 2010), since BF$^+$ is isoelectronic with these two molecular systems. We note that while there is no experimental data available for the processes considered here for BF$^+$, our previous calculation on N$_2^+$ and CO$^+$ gave good agreement with the available measurements.

References

Agarwal A and Kushner M 2007 *J. App. Phys,* **101** 063305

Amitay Z, Baer A, Dahan M, Levin J, Vager Z, Zajfman D, Knoll L, Lange M, Schwalm D, Wester R, Wolf A, Schneider I F, and Suzor-Weiner A 1999 *Phys. Rev. A* **60** 3769

Carr J M, Galiatsatos P G, Gorfinkiel J D, Harvey A G, Lysaght M A, Madden D, Masin Z, Plummer M and Tennyson J 2012 *Eur. Phys. J. D* **66** 58

Chakrabarti K and Tennyson J 2009 *J. Phys. B: At. Mol. Opt. Phys.* **42** 105204

Chakrabarti K, Schneider I F and Tennyson J 2011 *J. Phys. B: At. Mol. Opt. Phys.* **44** 055203

Epée Epée M D, Mezei J Zs, Motapon O, Pop N and Schneider I F 2015 *MNRAS* **455** 276

Farber M and Srivastava R D 1984 *J. Chem. Phys.* **81** 241–244

Florescu A I, Ngassam V, Schneider I F, and Suzor-Weiner A 2003, J. Phys. B **36** 1205

Giusti-Suzor A 1980 *J. Phys. B: At. Mol. Phys.* **13** 3867

Giusti-Suzor A, Bardsley J. N and Derkits C 1983 *Phys. Rev. A* **28** 682-691

Greene C H and Jungen C 1985 *Adv. At. Mol. Phys.* **21** 51

Guberman S L 2000 *in* M Larsson, J B A Mitchell and I F Schneider, eds., *Dissociative Recombination: Theory, Experiment and Applications IV*, World Scientific Singapore p. 111

Guberman S L and Giusti-Suzor A 1991 *J. Chem. Phys.* **95** 2602

Jungen C 1996, ed., *Molecular Applications of Quantum Defect Theory*, Institute of Physics Publishing Bristol

Jungen Ch 2011, "Elements of quantum defect theory", in *Handbook of High Resolution Spectroscopy*, edited by Quack M and Merkt F, Wiley, Chichester, New York

Jungen C and Atabek O 1977 *J. Chem. Phys.* **66** 5584

Kim Y-K and Irikura K 2000 *AIP Conf. Proc.* **543** 220–241

Kokoouline V, Greene C H and Esry B D 2001 *Nature* **412** 891

Kokoouline V and Greene C H 2003 *Phys. Rev. A* **68** 012703 B R 2007 *Mol. Phys.* **105** 1625

Lepers M and Dulieu O 2011 *Eur. Phys. J. D* **65** 113

Little D A, Chakrabarti K, Mezei J Zs, Schneider I F & Tennyson J 2014 *Phys. Rev. A* **90** 052705

Ilias Magoulas I, Kalemos A and Mavridis A 2013 *J. Chem. Phys.* **138** 104312

Matsui T, Kondo M and Matsuda A 2004 *Journal of Non-crystalline Solids* **338** 646–650

Maury M, Torregrosa F, Borvon G and Hassouni K 2016 *To be submitted to Plasma Chemistry and Plasma Processing*

Medved M, Fowler P W, and Hutson J M 2000 *Mol. Phys.* **98** 453

Mezei J Zs, Schneider I F, Roueff E and Jungen Ch 2012 *Phys. Rev. A* **85** 043411

Mezei J Zs, Schneider I F, Glass-Maujean M and Jungen Ch 2012 *J. Chem. Phys.* **141** 064305

Mezei J Zs, Backodissa-Kiminou R B, Tudorache D E, Morel V, Chakrabarti K, Motapon O, Dulieu O, Robert J, Tchang-Brillet W-Ü L, Bultel A, Urbain X, Tennyson J, Hassouni K and Schneider I F 2015 *Plasma Sources Sci. Technol.* **24** 035005

Motapon O, Fifirig M, Florescu A, Waffeu Tamo F O, Crumeyrolle O, Varin-Bréant G, Bultel A, Vervisch P, Tennyson J and Schneider I F 2006 *Plasma Sources Sci. Technol.* **15** 23

Motapon O, Pop N, Argoubi F, Mezei J Zs, Epee Epee M D, Faure A, Telmini M, Tennyson J and Schneider I F 2014 *Phys Rev. A* **90** 012706

Ngassam V, Motapon O, Florescu A, Pichl L, Schneider I F and Suzor-Weiner A 2003a *Phys. Rev. A* **68** 032704

Ngassam V, Florescu A, Pichl L, Schneider I F, Motapon O, and Suzor-Weiner A 2003b *Eur. Phys. J. D* **26** 165

Kramida O, Ralchenko Yu, Reader J, and NIST ASD Team 2015 NIST Atomic Spectra Database (ver. 5.3), National Institute of Standards and Technology, Gaithersburg, MD., `http://physics.nist.gov/asd`

Pop N, Lique F and Schneider I F 2012 *AIP Conf. Proc.* **1472** 162

Schneider I F, Pop N and Jungen Ch 2012 *Phys. Rev. A* **86** 062706

Roos J B, Orel A E and Larson Å 2009 *Phys. Rev. A* **79** 062510

Sarpal B K, Branchett S E, Tennyson J & Morgan L A 1991 *J. Phys. B: At. Mol. Opt. Phys.* **24** 3685–3699.

Schneider I F, Strömholm C, Carata L, Urbain X, Larsson M and Suzor-Weiner A 1997 *J. Phys. B: At. Mol. Opt. Phys.* **30** 2687

Schneider I F, Dulieu O and Giusti-Suzor A 1991 *J. Phys. B: At. Mol. Phys.* **24** L289

Schneider I F, Rabadan, L I, Carata L, Tennyson J, Andersen A H an Suzor-Weiner A 2000a *J. Phys. B: At. Mol. Opt. Phys.* **33** 4849

Schneider I F, Orel A E and Suzor-Weiner A 2000b *Phys. Rev. Lett.* **85** 3785

Seaton M J 1983 *Rept. Prog. Phys.* **46** 167

Sidis V and Lefebvre-Brion H 1971 *J. Phys. B* **4** 1040

Sommavilla M, Merkt F, Mezei J Zs and Jungen Ch 2016 *J. Chem. Phys.* **144** 084303

Stone A J 1996 *The Theory of Intermolecular Forces*, New York: Oxford University Press

Sun H and Nakamura H 1990 *J. Chem. Phys.* **93** 6491

Takagi H 1993 *J. Phys. B: At. Mol. Opt. Phys.* **26** 4815

Tanabe T, Katayama I, Kamegaya H, Chida K, Arakaki Y, Watanabe T, Yoshizawa M, Saito M, Haruyama Y, Hosono K, Hatanaka K, Honma T, Noda K, Ohtani S and Takagi H 1995 *Phys. Rev. Lett.* **75** 1066

Tennyson J and Noble C J 1984 *Comput. Phys. Commun.* **33** 421–424

Tennyson J 2010 *Phys. Rep.* **491** 29-76.

Torregrosa F, Laviron C, Faik H, Barakel D, Milesi F and Baccaccia S 2004 *Surface & Coatings Technology* **186** 93–98

Vâlcu B, Schneider I F, Raoult M, Strömholm C, Larsson M and Suzor-Weiner A 1998 *European Physical Journal D* **1** 71

Yamamoto H, Matsumoto S, Okada K, Yu J and Hirakuri K 2006 *Diamond and Related Materials* **15** 1357–1361

Yu J and Matsumoto S 2003 *Diamond and Related Materials* **12** 1903–1907